Journal of Materials Chemistry

Cite this: DOI: 10.1039/c1jm11266j

www.rsc.org/materials

PAPER

Partially oxidized graphene as a precursor to graphene†

Goki Eda,[a] James Ball,[b] Cecilia Mattevi,[a] Muge Acik,[c] Luca Artiglia,[d] Gaetano Granozzi,[d] Yves Chabal,[c] Thomas D. Anthopoulos[b] and Manish Chhowalla‡*[a]

Received 24th March 2011, Accepted 19th May 2011
DOI: 10.1039/c1jm11266j

Solution exfoliation of graphite holds promise for large-scale bulk synthesis of graphene. Non-covalent exfoliation is attractive because the electronic structure of graphene is preserved but the yield is low and the lateral dimensions of the sheets are small. Chemical exfoliation *via* formation of graphite oxide is a highly versatile and scalable route but the covalent functionalization of graphene with oxygen significantly alters the properties. Here, we report a new method for large-scale facile synthesis of micron-sized partially oxidized graphene (POG) sheets with dramatically improved electronic properties compared to other solution-phase exfoliated graphene. Due to low initial oxygen content (~12%), POG requires only mild annealing (<300 °C) to achieve a sheet resistance of 28 kΩ sq^{-1} at the neutrality point, only a factor of ~4 larger than the intrinsic sheet resistance of pristine graphene (~6 kΩ sq^{-1}) and substantially lower than graphene exfoliated by other methods. Such a partial oxidation approach opens up new promising routes to solution based high-performance, low temperature, transparent and conducting graphene-based flexible electronics.

Introduction

Bulk production of graphene from chemical exfoliation of graphite is required for applications where a large volume of material is required.[1,2] While a number of exfoliation schemes have been proposed,[1] none has been found to yield graphene with electrical properties comparable to those of chemical vapor deposited, silicon carbide converted or mechanically exfoliated graphene. Exfoliation of graphite *via* graphite oxide has been widely studied due to high yield of monolayer sheets, graphene oxide (GO), with lateral dimensions up to a few to hundreds of microns that are soluble in common solvents such as water.[3–5] As-synthesized GO is insulating but can be reduced to obtain intrinsic sheet resistance of 1 MΩ sq^{-1}, a few orders of magnitude larger than that of pristine graphene (~6 kΩ sq^{-1}). Other chemical routes utilize organic molecules or surfactants to intercalate into graphite and non-covalently bind to graphene surface[6–8] to achieve exfoliation. However such methods must be assisted by prolonged ultrasonication that tends to fragment the graphene sheets into submicron lateral dimensions that significantly deteriorates the properties of large-area thin films.[6,7,9] A scalable method to high quality graphene with large lateral sizes is therefore currently lacking.

The electronic quality of reduced GO (rGO) is limited mainly by residual oxygen functional groups[10] and structural defects that originate from loss of carbon from the basal plane in the form of CO and CO_2 during reduction.[11–13] Thus, efficient removal of oxygen and suppression of defect-forming mechanisms are crucial for achieving the highest electronic quality rGO. While some progress has been made towards this end,[14] most studies indicate that high carrier mobilities are achieved only after high temperature (~1000 °C) reduction,[15–18] often in conjunction with prior chemical treatment such as exposure to hydrazine vapor.[19] However, even after high temperature treatments,[20] a significant amount of oxygen is present in various stable forms.[20,21] A recent study showed that in highly oxidized samples, oxygen functional groups in close proximity interact to form stable species such as in-plane ether or out-of-plane carbonyl groups.[21] The formation of stable defect species can be avoided in samples with lower initial oxygen content because isolated functional groups such as hydroxyls desorb directly, leaving the graphene basal plane intact. When typical oxidation process such as the modified Hummers or Brodie's method is used, GO is fully oxidized with an oxygen content of ~30%. A few recent studies[22–25] have suggested that exfoliation of mildly oxidized graphite could lead to graphene sheets with improved properties. However, small size and yield have limited extensive investigation of properties and chemistry and efficient reduction mechanisms remain elusive.

[a]*Department of Materials, Imperial College London, Exhibition Road, London, SW7 2AZ, UK. E-mail: manish1@rci.rutgers.edu*
[b]*Department of Physics and Centre for Plastic Electronics, Blackett Laboratory, Imperial College London, Exhibition Road, London, SW7 2BW, UK*
[c]*Department of Materials Science and Engineering, The University of Texas at Dallas, Richardson, Texas, 75080, USA*
[d]*Department of Chemical Science, University of Padova, Via Marzolo 1, I-35131 Padova, Italy*

† Electronic supplementary information (ESI) available. See DOI: 10.1039/c1jm11266j

‡ Present address: Materials Science and Engineering, Rutgers University, 607 Taylor Road, Piscataway, New Jersey 08854, USA.

Here, we report a simple scalable synthesis of partially oxidized graphene (POG) which exhibits electrical properties that are distinctly superior to those of graphene derived from other solution-phase exfoliation methods. We show that mild oxidation of graphite followed by intercalation with tetrabutylammonium hydroxide (TBA) leads to a highly stable colloidal dispersion of POG flakes with lateral dimensions that are larger than those obtained by non-covalent exfoliation methods.[6–8] These POG sheets have an initial oxygen content of only 12% and exhibit a chemical structure that is distinctly different from all other forms of chemically derived graphene reported in the literature. We demonstrate that POG can be efficiently reduced at low temperatures (<300 °C) to achieve high electrical conductivity. We describe the structural, chemical, and electronic properties of POG in detail and compare them to the well characterized fully oxidized GO to highlight the superior nature of POG.

Experimental section

Material synthesis

The oxidation method utilized in this study is based on Brodie's method.[26] All chemicals were obtained from Sigma-Aldrich and used without further purification. Natural graphite (0.5 g) was immersed in concentrated nitric acid (10 mL). Potassium chlorate (5 g) was slowly added into the mixture while the temperature was maintained around room temperature. The reacted graphite was washed with a copious amount of water to remove the acid, oxidant, and any fully oxidized GO which is soluble in water. For comparison, fully oxidized GO was synthesized *via* a modified Hummers method.[27] The mildly oxidized graphite was then intercalated with a tetrabutylammonium hydroxide (TBA) solution[28] (2 mL, 40% in water) in 20 mL dimethylformamide (DMF) at 80 °C for 5 days. The mixture was allowed to cool to room temperature and the POG sheets were precipitated out and the TBA was removed. The sediments were redispersed in fresh DMF. The final dispersion contained predominantly monolayers of POG and remained stable over several months with minimal precipitation.

Thin film deposition

Thin films of POG were prepared using Langmuir–Blodgett (L–B) assembly.[29] Briefly, a suspension of POG in DMF was carefully applied on a water surface dropwise. The suspension immediately spread over the water surface due to the high surface tension of water. After several droplets (~50 μL) were applied, a continuous film of monolayer POG was formed. Unlike in the conventional L–B deposition, the substrate was slowly brought into contact with the film from above the water surface and retracted. Excess water was carefully absorbed. This simple process yielded highly uniform films of monolayer POG transferred onto substrates from the air–water interface. Thicker films were prepared by repeating the above procedure.

Reduction

Reduction of POG was achieved by annealing the sample for 1 hour in a nitrogen atmosphere except in XPS and FTIR studies where the samples were annealed in vacuum. Unless stated otherwise, an annealing temperature of 250 °C was used. Chemical reduction of POG was conducted by using ascorbic acid (vitamin C) following a recently reported procedure.[30]

Characterization

X-Ray diffraction of partially oxidized graphite, GO paper, and pristine graphite was obtained under ambient condition in a PANalytical X'Pert Pro MPD with Cu K_α X-ray source. To minimize the effect of adsorbed water, the samples were dried over phosphorus pentoxide for ~3 days.

Transmission electron microscope (TEM) images were taken in a JEOL 2000X at 200 kV. The TEM samples were prepared by depositing POG flakes on holey carbon mesh using the L–B method described above. Field emission scanning electron microscope (SEM) images of POG deposited on SiO_2/Si substrates were obtained on a Gemini LEO1525 at 5 kV in inlens detection mode.

UV-visible absorption of POG thin films deposited on quartz substrates was measured by a PerkinElmer Lambda 25 UV-vis spectrometer under ambient condition.

In situ infrared absorption measurements (4 cm^{-1} resolution) were performed in transmission (~70° incidence) through two KBr-IR windows with a Nicolet Nexus 670 equipped with a DTGS detector. Si(100) wafers with ~6 to 7 nm of thermal oxide (CZ, n-type, double side polished with a nominal resistivity of 1–20 Ω cm) were cleaned by sequential rinsing in DI water (Nanopure deionized water with a resistivity of 18.2 MΩ cm and a total organic carbon (TOC) below 5 ppb obtained from a Millipore system), ethyl acetate, methanol, and DI water, and immersion in piranha solution (98% H_2SO_4/30% H_2O_2, 2 : 1, v/v) at 90 °C for at least 30 minutes and rinsed with copious amounts of DI water. ***Caution****: piranha solution is extremely corrosive and should be handled with care*. Single layer and three layers of POG films were then deposited on both sides of these clean SiO_2/Si substrates (1.5 × 3.8 cm) and measurements were performed at 60 °C in a vacuum chamber.

Micro-Raman spectra were obtained on a Jobin Yvon LabRam Infinity using 532 nm excitation. The excitation laser was focused on individual monolayer flakes of POG.

X-Ray photoelectron spectroscopy (XPS) data were taken on films deposited on Pt foils using a VG ESCALAB MK II (Vacuum generators, Hastings, England) system (base pressure of 1 × 10^{-7} Pa) equipped with a twin anode (Mg/Al) X-ray source with a hemispherical electrostatic analyzer with a five channeltrons detector. All the spectra reported were collected using Al K_α excitation energy. The binding energy (BE) calibration was carried out using the 4f peaks of the Pt foil. Spectra were taken at room temperature before and after annealing in vacuum without exposing the sample to air.

For evaluation of the electrical properties of POG films, bottom-gate, top-contact field-effect transistor (FET) structures were used. Measurements were conducted on a Keithley 4200 semiconductor parameter analyzer. Doped Si wafers served as both the supporting substrate and global gate electrode. The dielectric layer was 300 nm of thermally grown SiO_2 (geometrical capacitance, $C_i = 11.5$ nF cm^{-2}). A POG film was deposited onto the SiO_2 by L–B deposition as described above and devices were

completed by shadow mask evaporation of Au source and drain contact electrodes. All measurements were conducted on ~2 layer films with an apparent thickness of 2 nm unless otherwise noted. Devices with channel lengths (L) of 20–40 μm with a width (W) of 1000–1500 μm were tested and all devices showed similar behavior. For electrical characterization on individual POG flakes, Au electrodes were deposited initially on SiO_2/Si substrates and a sparse non-continuous layer of POG was deposited from solution. Devices with the channel region ($L = 1$ μm and $W = 1$ μm) fully covered by a single monolayer of POG flake were selected for subsequent characterization. Two-dimensional conductivity (σ) was calculated using $\sigma = 1/R_s$ where R_s is the sheet resistance measured by two-probe and four-probe methods (both yielding consistent values). The corresponding bulk conductivity was calculated using $\sigma_{bulk} = \sigma/t$ where t is the apparent thickness measured by AFM.

Results and discussion

Upon partial oxidation using the method described above, the interlayer spacing of graphite was found to have expanded slightly compared to the pristine material. The lateral size however remained largely unchanged indicating minimal etching of the graphite from the edges during oxidation (Fig. 1a). The X-ray diffraction spectrum of the oxidized powder shown in Fig. 1b clearly demonstrates the presence of the graphite oxide phase[31] at ~15° along with the residual graphite phase at ~26° (Fig. 1b). The absence of an amorphous phase background that is typically present in GO paper suggests higher degree of structural order in mildly oxidized graphite.

Visually, POG suspension is black with weak brown tint indicating that the aromatic network is largely preserved

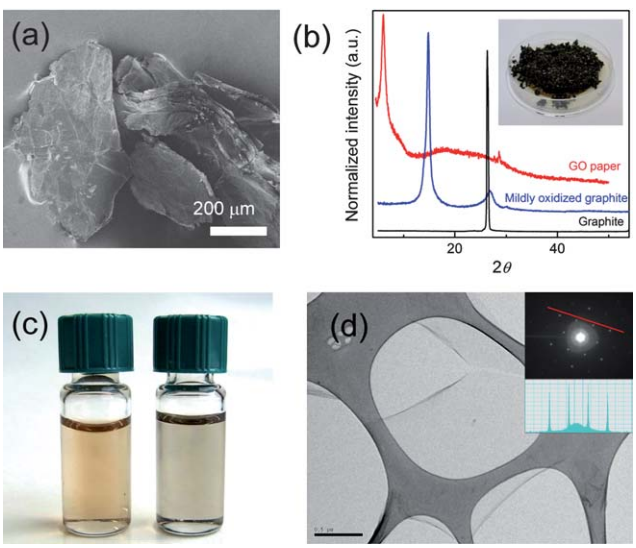

Fig. 1 (a) SEM image of partially oxidized graphite flakes. (b) X-Ray diffraction spectra of graphite, GO paper and partially oxidized graphite. The inset is a photograph of partially oxidized graphite powders. (c) Photograph of a suspension of GO in water (left) and POG in DMF (right) having similar optical density. (d) TEM image of a monolayer POG suspended over holey carbon grid. The inset shows a SAED pattern taken at the center of the POG sheet and the corresponding intensity profile along the line shown.

(Fig. 1c). This is in contrast with the GO suspension, which is brownish in appearance. Exfoliation of partially oxidized and intercalated graphite was less efficient compared to graphite oxide prepared through the modified Hummers method. Nevertheless, the yield of our method is estimated to be a few weight percent, and results in concentrated (~1 mg mL^{-1}) suspensions of mono- and few-layer POG. Electron diffraction patterns of POG sheets comprise of a single set of hexagonal patterns similar to those commonly observed in monolayer graphene[32] and GO[33] (Fig. 1d). The relative intensity of the inner $1\bar{1}00$-type reflections and outer $2\bar{1}\bar{1}0$-type reflections further confirm that the flakes are monolayers of POG (Fig. 1d, inset).

The SEM image of a single LB deposition in Fig. 2a shows a highly uniform coverage by densely packed POG sheets covering >90% of the substrate surface. The POG sheets were distinctly smaller than the oxidized graphite with the majority of the sheets having a lateral size of between 3 and 10 μm suggesting that tearing of the sheets occurred during the intercalation or the exfoliation process. We note that a uniform deposition was achieved over areas as large as 5 cm^2 under non-optimized conditions. Minimal overlap between the sheets suggests the presence of repulsive electrostatic forces among the edge functional groups.[29] The majority of the sheets (~90%) were found to be monolayers having a thickness of about 1 nm (see ESI† for AFM results) and the rest were multilayers (seen as darker regions in Fig. 2a). Multiple depositions lead to layer-by-layer deposition as shown in Fig. 2b and c. POG was found to be slightly more hydrophobic compared to GO with clear difference in contact angles (~60° and ~50° for 2-layer films of POG and GO, respectively), implying lower concentration of polar oxygen functional groups in POG (Fig. 2d and e).

The absorption spectrum of as-synthesized POG thin films shows that the peak related to the π–π* transitions is red-shifted compared to that of GO thin films (Fig. 3a), indicating that it is oxidized to a lesser degree.[30,34] A red shift is observed in POG after thermal reduction, suggesting removal of oxygen. It can also be noticed that the GO peak arising from n → p* transitions of C=O at 300–310 nm is significantly diminished in POG, indicating low concentration of carbonyl and carboxyl groups.

The infrared absorbance spectra shown in Fig. 3a provide further evidence that the chemical structures of as-synthesized and reduced single layer POG are significantly different from those of single layer GO. The vibrational modes corresponding to POG and rPOG are mainly contributions from the ether groups (C–O, 800–1200 cm^{-1}) and sp^2-hybridized C=C (1500–1600 cm^{-1}) vibrations with weak infrared intensity. Interestingly, absorption features associated with carbonyl (1750–1850 cm^{-1}), carboxyl (1650–1750 cm^{-1}), epoxide (1230–1330 cm^{-1}) and hydroxyl (3050–3800 cm^{-1}) groups, which are prominent in the spectrum for GO, are significantly diminished or absent for POG and rPOG. These results demonstrate that POG prepared by our method is distinctly different from mildly oxidized graphene samples reported by other groups.[22–25] The peaks at 3000–3500 cm^{-1} could be attributed to the stretching vibrational modes of C–H and at 3500–3800 cm^{-1} to N–H vibrations with additional contributions in the region of ~800 to 1500 cm^{-1} for stretching modes of C–N and bending modes of N–H and C–H, which is a possible indication of hydrolyzed DMF (*i.e.* formic acid and dimethylamide). After annealing, the peaks for ethers

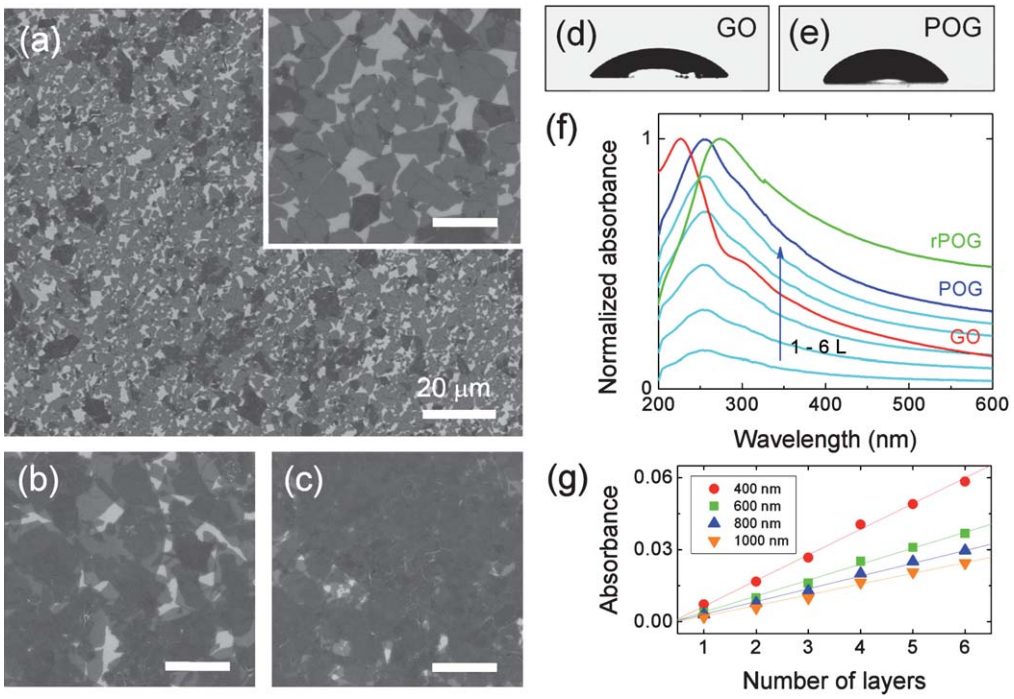

Fig. 2 (a) SEM image of a monolayer POG film deposited on a SiO_2/Si substrate *via* L–B assembly. The inset shows a higher magnification image (scale bar: 6 μm). The dominant grey and dark grey regions correspond to monolayer and multilayer POG sheets, respectively. The substrate surface appears as light grey. (b) and (c) are SEM images of 2 layer and 3 layer POG film, respectively (scale bar: 6 μm). (d and e) Photograph of a water droplet on 2-layer (d) GO and (e) POG films showing slightly higher contact angle for POG. (f) Normalized UV-visible absorbance of GO, POG, and rPOG films. The plots for GO, rPOG, and 6-layer POG are normalized at the peak value. The data for 1- to 6-layer POG are plotted keeping the experimentally observed relative intensity. (g) Absorbance of POG films as a function of the number of layers at different wavelengths.

and/or epoxides and C–H were diminished, indicating reduction and removal of some organic residues on the samples. The presence of a C=C peak, which requires nearby functional groups to be activated, implies that some residual oxygen is present in the sample after mild annealing.

The Raman spectra of POG consist mainly of prominent D and G peaks and weak 2D and D + G peaks. Close examination of the D and 2D peaks reveals that the FWHM is ~20% wider for GO, suggesting greater disorder. The D/G peak ratios do not correlate well with the electronic quality of rGO.[10,35] The correlation length, L_a, or size of the defect-free sp^2 carbon clusters, can be estimated by $L_a^2C'(\lambda) = I(D)/I(G)$ where $I(D)$ and $I(G)$ are Raman intensity of the D and G peaks, respectively, and $C'(\lambda)$ is a constant dependent on excitation laser wavelength.[36] The lower bound of the sp^2 carbon cluster size in POG can be estimated using this relationship. Taking the $I(D)$ and $I(G)$ of GO and POG, L_a for POG is estimated to be at least 2.8 times greater than that of GO. Erickson *et al.*[37] recently showed with high resolution TEM analysis that the sp^2 carbon clusters of GO range between 1 and 6 nm^2 in size, in good agreement with earlier studies.[38,39] If we assume the average sp^2 carbon cluster area in GO to be ~3 nm^2, then we can estimate the cluster size in POG to be greater than ~24 nm^2, consistent with the low initial oxygen content. However, careful high resolution TEM study is necessary to verify this result. It is worth noting that a slight increase in the D peak was observed after thermal reduction of POG suggesting formation of some defects during desorption of functional groups in a manner similar to GO.

The C1s peak region in the XPS spectra was deconvoluted to the components which are expected to be present in the samples.[10,40] Specifically, these are: C sp^2 in aromatic rings (284.6 eV); C–O (286.1 eV); C=O (287.5 eV); C(=O)–(OH) (289.2 eV); and π–π* satellite peak (290.6 eV) (Fig. 4a). In contrast to GO where the C–O component is typically comparable to C sp^2 in intensity, as-synthesized POG shows significantly weaker C–O and C=O, in good agreement with the FTIR results. These components further diminished after mild annealing. The oxygen contents in POG and rPOG reduced at 300 °C were found to be 12 and 3%, respectively. The onset of reduction was found to occur between 100 and 200 °C, similar to the case of GO[10,40] (Fig. 4b and c). For comparison, measurements conducted under identical conditions for GO yielded ~40% and ~15% for as-synthesized GO and rGO reduced at 300 °C. It should be noted that even at a reduction temperature of 1000 °C, an oxygen content of 3% cannot not be achieved in GO.[10] The total sp^2 carbon content accounting for defect-induced peak shift for POG reduced at 300 °C was found to be 90–92%, which is higher than the values for GO reduced at 1000 °C.

As-synthesized GO is an electrical insulator with a large sheet resistance of ~10^{12} Ω sq^{-1}.[19] As-synthesized POG was found to be conducting with a sheet resistance of ~10^9 Ω sq^{-1}. In FET configuration, POG also exhibited the typical ambipolar field effect with gate bias (Fig. 5a). The field-effect mobility (μ) was extracted from the drain current (I_D) as a function of gate voltage above the threshold ($V_G - V_T$) voltage assuming $I_D = (\mu C_i W/L)$

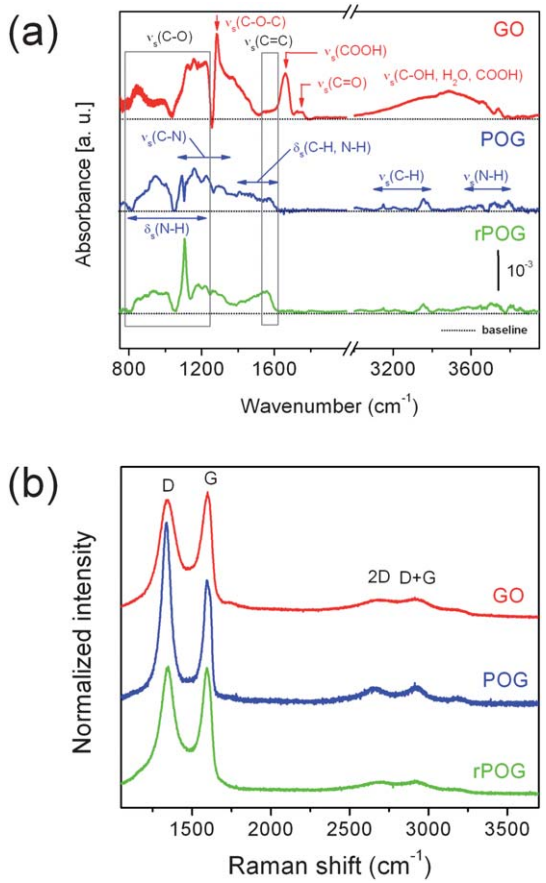

Fig. 3 (a) *In situ* FTIR absorbance spectra in transmission and (b) Raman spectrum (excitation wavelength: 532 nm) for GO, POG and rPOG thin films. The noise-like features around 1000 cm^{-1} in (a) arise from the TO phonon modes of the Si substrate.

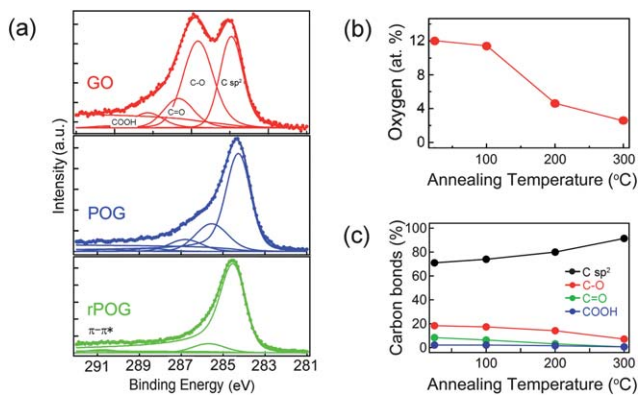

Fig. 4 (a) C1s region of the XPS spectrum for GO, POG and rPOG. The spectra were deconvoluted to 5 components as described in the text. (b) Atomic oxygen concentration of POG as a function of annealing temperatures. (c) Percent fraction of sp^2 carbon, C–O, C O, and COOH as a function of the annealing temperatures.

$[(V_G - V_T) - V_D^2/2]$ for an FET with channel length L and width W at a fixed drain voltage (V_D). The mobility in as-synthesized POG thin films was found to be on the order of 10^{-4} cm^2 V^{-1} s^{-1} and typically higher for holes than electrons. As shown in Fig. 5e, mobility was found to increase almost linearly with increasing lateral field (E_D). The origin of such behavior is not clear, however, since defects such as oxygen functional groups can be trapping centers, a Poole–Frenkel type electrical conduction mechanism, where charge carriers are de-trapped by field-assisted activation, is likely to play an important role.

After annealing at 250 °C, the conductivity of POG films improved by ~5 orders of magnitude reaching ~10 μS with the corresponding bulk conductivity of 50 S cm^{-1}. Field modulation of channel conductance was significantly suppressed indicating an evolution of the electronic structure and trap state distribution of POG[41] (Fig. 5b). The low on/off behavior of rPOG may be attributed to increase in density of states (DOS) near Fermi energy due to defects[41] and also to the presence of charged impurities on the substrate surface.[15] The field-effect mobility of rPOG thin films was around 1–3 cm^2 V^{-1} s^{-1} and was found to be nearly independent of lateral fields (Fig. 5f). This indicates that a large proportion of residual trap states is thermally accessible such that the influence of field is greatly diminished. Improvement in both electrical conductivity and mobility by a factor of 2–4 was observed when POG was chemically reduced prior to annealing (Fig. 5c and g). Optimum reduction leads to a sheet resistance of 28 kΩ sq^{-1} at the neutrality point for individual monolayer rPOG, which is only a factor of ~4 larger than the intrinsic sheet resistance of pristine graphene.[42] The conductivity and mobility of individual monolayer rPOG sheets were found to be higher than those of corresponding 1 layer films by a factor of 2–4. This result is consistent with the recent report which indicated the detrimental effects of inter-sheet junctions in carrier transport.[43]

For low reduction temperatures, the sheet resistance of rPOG films was found to be more than one order of magnitude lower than that of rGO films with similar thicknesses and optical transparency. However, after high temperature reduction (~1000 °C), both rPOG and rGO exhibited similar sheet resistance and transparency. These observations suggest that carrier transport in these films is not only limited by the residual oxygen functional groups and defects but also by other factors such as inter-sheet resistance and charged impurities (see ESI† for details).

Field effect mobilities obtained from POG and GO with various reduction conditions are summarized in Fig. 6. The upper panel shows the results for ~2 layer film from the current study. In the bottom panel, the result for individual POG is compared with previously reported results on individual flakes of GO reduced in various conditions.[16,18,35,41] It can be seen that the chemically reduced POG without subsequent annealing exhibits mobilities comparable to those of GO reduced at 250 °C. For identical annealing conditions, POG films exhibited one order of magnitude higher mobilities compared to GO. It should be noted that the properties of GO and POG thin films are influenced by various factors such as flake size and film morphology. The average sheet sizes particularly become critical for high mobility devices because carrier mobility is expected to be limited by sheet-to-sheet junctions. In this study, the POG sheets were 5–6 times smaller than the GO sheets in lateral size. Thus it is remarkable that despite the smaller size of the POG sheets, large mobilities were observed.

Electrical properties of individual POG and GO sheets provide a better comparison because effects of flake size and

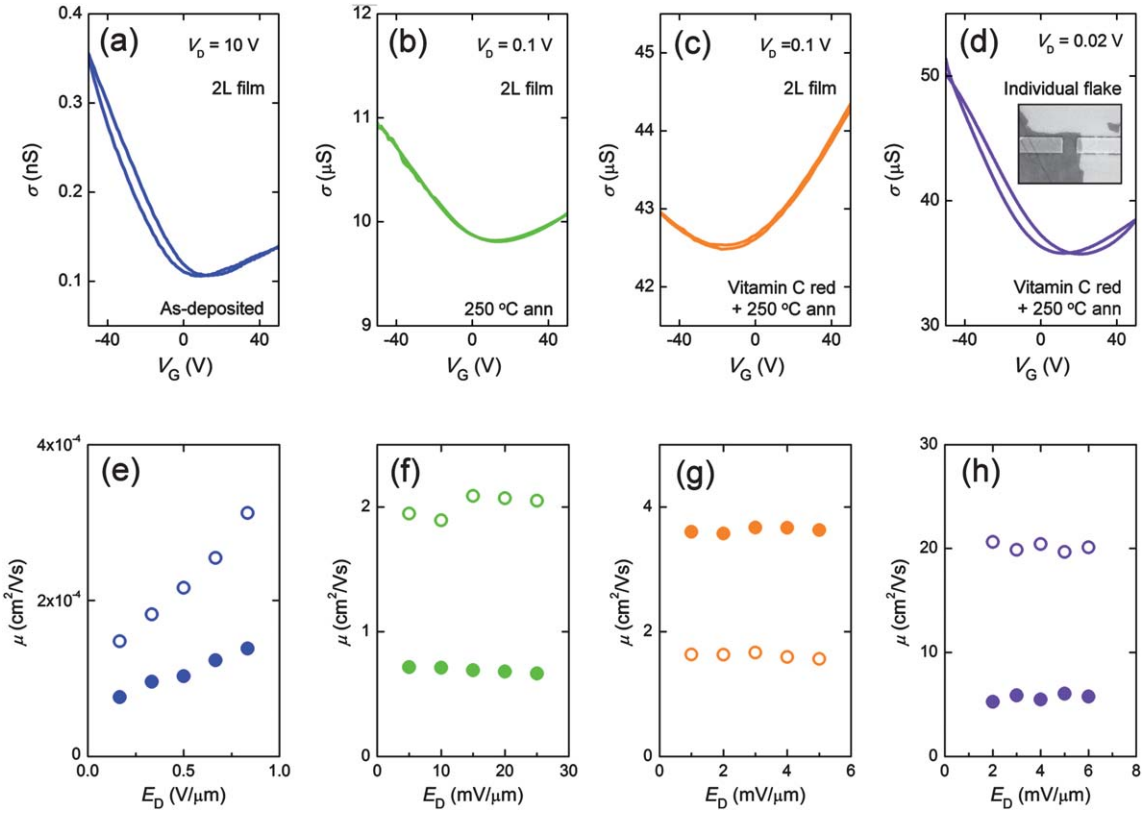

Fig. 5 Transfer characteristics of (a) POG, (b) thermally reduced POG, and (c) chemically and thermally reduced POG thin films. (d) Transfer characteristics of a single flake of chemically and thermally reduced POG. (e–h) Field effect mobility as a function of source-drain electric field corresponding to the devices in (a–d), respectively. "red" and "ann" stand for "reduction" and "annealing", respectively.

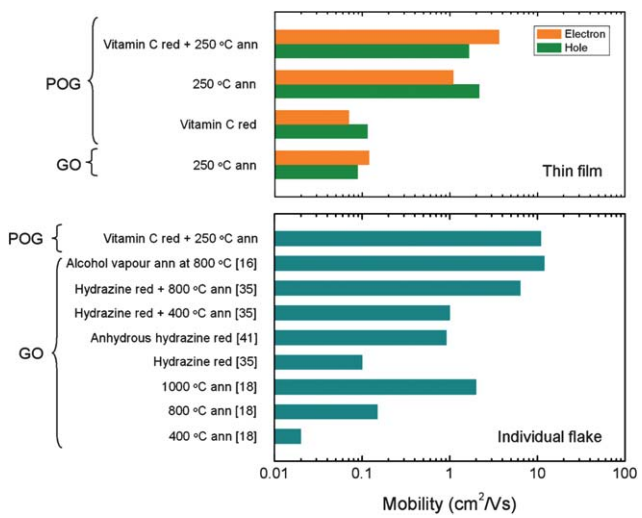

Fig. 6 Summary of field effect mobilities of rGO and rPOG reduced at different conditions. Some results for GO were taken from ref. 16,18,35 and 41 for comparison. "red" and "ann" stand for "reduction" and "annealing", respectively. The top and the bottom panel summarize the results for thin film samples and individual flakes, respectively. In the bottom panel, the mobilities for the dominant carriers are reported.

morphological features can be eliminated. Surprisingly, mobilities obtained for rPOG that were chemically reduced and annealed at 250 °C are comparable to or significantly higher than those of rGO that have been reduced at much higher temperatures.[16,18,35] These results indicate that mild annealing of POG is sufficient to achieve an extended network of sp^2 carbon that is comparable to that of highly reduced GO.

Conclusions

We have demonstrated that graphite can be exfoliated into individual sheets *via* mild oxidation followed by intercalation. By minimizing the aggressive oxidation process commonly employed in many studies and avoiding prolonged ultrasonication, large sheets (>1 μm) of POG can be obtained. The chemistry of POG was found to be distinctly different from that of GO. The main oxygen functional groups were in the form of epoxide and/or ethers and other groups such as carboxyl, carbonyl, and hydroxyl were present in only minor concentrations in POG. Due to the low initial concentration of oxygen (~12%), as-synthesized POG is conductive in contrast to as-synthesized GO which is highly insulating. Low sheet resistance (~28 kΩ sq^{-1}) can be achieved in individual monolayer rPOG after mild annealing (<300 °C) due to efficient reduction. POG allows fabrication of devices at temperatures significantly lower than that required to achieve equivalent reduction in GO even without the need for reducing chemicals. Our results offer a promising route towards incorporating chemically derived graphene into a variety of materials systems where low temperature processing is desired.

Acknowledgements

We thank Prof. Bill Milne's group at University of Cambridge for lithographic patterning of some devices. We acknowledge the financial support from Centre for Advanced Structural Ceramics (CASC) at Imperial College London. G.E. acknowledges the Royal Society for the Newton International Fellowship. M.C. acknowledges support from the Royal Society through the Wolfson Merit Award. The work at the University of Texas at Dallas was supported by the SWAN-NRI Program and Texas Instruments.

References

1 S. Park and R. S. Ruoff, *Nat. Nanotechnol.*, 2009, **4**, 217.
2 K. P. Loh, Q. Bao, P. K. Ang and J. Yang, *J. Mater. Chem.*, 2010, **20**, 2277.
3 S. Stankovich, D. A. Dikin, R. D. Piner, K. A. Kohlhaas, A. Kleinhammes, Y. Jia, Y. Wu, S. T. Nguyen and R. S. Ruoff, *Carbon*, 2007, **45**, 1558.
4 G. Eda and M. Chhowalla, *Adv. Mater.*, 2010, **22**, 2392.
5 K. P. Loh, Q. Bao, G. Eda and M. Chhowalla, *Nat. Chem.*, 2010, **2**, 1015.
6 Y. Hernandez, V. Nicolosi, M. Lotya, F. M. Blighe, Z. Sun, S. De, I. T. McGovern, B. Holland, M. Byrne, Y. K. Gun'Ko, J. J. Boland, P. Niraj, G. Duesberg, S. Krishnamurthy, R. Goodhue, J. Hutchison, V. Scardaci, A. C. Ferrari and J. N. Coleman, *Nat. Nanotechnol.*, 2008, **3**, 563.
7 M. Lotya, Y. Hernandez, P. J. King, R. J. Smith, V. Nicolosi, L. S. Karlsson, F. M. Blighe, S. De, Z. Wang, I. T. McGovern, G. S. Duesberg and J. N. Coleman, *J. Am. Chem. Soc.*, 2009, **131**, 3611.
8 X. An, T. Simmons, R. Shah, C. Wolfe, K. M. Lewis, M. Washington, S. K. Nayak, S. Talapatra and S. Kar, *Nano Lett.*, 2010, **10**, 4295.
9 P. Blake, P. D. Brimicombe, R. R. Nair, T. J. Booth, D. Jiang, F. Schedin, L. A. Ponomarenko, S. V. Morozov, H. F. Gleeson, E. W. Hill, A. K. Geim and K. S. Novoselov, *Nano Lett.*, 2008, **8**, 1704.
10 C. Mattevi, G. Eda, S. Agnoli, S. Miller, K. A. Mkhoyan, O. Celik, D. Mastrogiovanni, G. Granozzi, E. Garfunkel and M. Chhowalla, *Adv. Funct. Mater.*, 2009, **19**, 2577.
11 I. Jung, D. A. Field, N. J. Clark, Y. Zhu, D. Yang, R. D. Piner, S. Stankovich, D. A. Dikin, H. Geisler, C. A. Ventrice and R. S. Ruoff, *J. Phys. Chem. C*, 2009, **113**, 18480.
12 M. Acik, C. Mattevi, C. Gong, G. Lee, K. Cho, M. Chhowalla and Y. J. Chabal, *ACS Nano*, 2010, **4**, 5861.
13 M. Acik, R. Guzman and Y. J. Chabal, *Mater. Res. Soc. Symp. Proc.*, 2010, **1205E**, L01.
14 W. Gao, L. B. Alemany, L. Ci and P. M. Ajayan, *Nat. Chem.*, 2009, **1**, 403.
15 S. Wang, P. K. Ang, Z. Wang, A. L. L. Tang, J. T. L. Thong and K. P. Loh, *Nano Lett.*, 2010, **10**, 92.
16 C.-Y. Su, Y. Xu, W. Zhang, J. Zhao, A. Liu, X. Tang, C.-H. Tsai, Y. Huang and L.-J. Li, *ACS Nano*, 2010, **4**, 5285.
17 D. C. Marcano, D. V. Kosynkin, J. M. Berlin, A. Sinitskii, Z. Sun, A. Slesarev, L. B. Alemany, W. Lu and J. M. Tour, *ACS Nano*, 2010, **4**, 4806.
18 X. Dong, C.-Y. Su, W. Zhang, J. Zhao, Q. Ling, W. Huang, P. Chen and L.-J. Li, *Phys. Chem. Chem. Phys.*, 2010, **12**, 2164.
19 H. A. Becerril, J. Mao, Z. Liu, R. M. Stoltenberg, Z. Bao and Y. Chen, *ACS Nano*, 2008, **2**, 463.
20 M. Acik, G. Lee, C. Mattevi, M. Chhowalla, K. Cho and Y. J. Chabal, *Nat. Mater.*, 2010, **9**, 840.
21 A. Bagri, C. Mattevi, M. Acik, Y. J. Chabal, M. Chhowalla and V. B. Shenoy, *Nat. Chem.*, 2010, **2**, 581.
22 S. Wang, P.-J. Chia, L.-L. Chua, L.-H. Zhao, R.-Q. Png, S. Sivaramakrishnan, M. Zhou, R. G. S. Goh, R. H. Friend, A. T. S. Wee and P. K. H. Ho, *Adv. Mater.*, 2008, **20**, 3440.
23 X. Li, G. Zhang, X. Bai, X. Sun, X. Wang, E. Wang and H. Dai, *Nat. Nanotechnol.*, 2008, **3**, 538.
24 P. K. Ang, S. Wang, Q. Bao, J. T. L. Thong and K. P. Loh, *ACS Nano*, 2009, **3**, 3587.
25 J. Meihua, J. Hae-Kyung, Y. Woo Jong, B. Dong Jae, K. Bo Ram and L. Young Hee, *J. Phys. D: Appl. Phys.*, 2009, **42**, 135109.
26 B. C. Brodie, *Philos. Trans. R. Soc. London*, 1959, **149**, 249.
27 M. Hirata, T. Gotou and M. Ohba, *Carbon*, 2005, **43**, 503.
28 Z.-h. Liu, Z.-M. Wang, X. Yang and K. Ooi, *Langmuir*, 2002, **18**, 4926.
29 L. J. Cote, F. Kim and J. Huang, *J. Am. Chem. Soc.*, 2008, **131**, 1043.
30 M. J. Fernández-Merino, L. Guardia, J. I. Paredes, S. Villar-Rodil, P. Solís-Fernández, A. Martínez-Alonso and J. M. D. Tascón, *J. Phys. Chem. C*, 2010, **114**, 6426.
31 H. K. Jeong, M. H. Jin, K. P. So, S. C. Lim and Y. H. Lee, *J. Phys. D: Appl. Phys.*, 2009, **42**, 065418.
32 J. C. Meyer, A. K. Geim, M. I. Katsnelson, K. S. Novoselov, T. J. Booth and S. Roth, *Nature*, 2007, **446**, 60.
33 N. R. Wilson, P. A. Pandey, R. Beanland, R. J. Young, I. A. Kinloch, L. Gong, Z. Liu, K. Suenaga, J. P. Rourke, S. J. York and J. Sloan, *ACS Nano*, 2009, **3**, 2547.
34 D. Li, M. B. Müller, S. Gilje, R. B. Kaner and G. G. Wallace, *Nat. Nanotechnol.*, 2008, **3**, 101.
35 C.-Y. Su, Y. Xu, W. Zhang, J. Zhao, X. Tang, C.-H. Tsai and L.-J. Li, *Chem. Mater.*, 2009, **21**, 5674.
36 A. C. Ferrari and J. Robertson, *Phys. Rev. B: Condens. Matter Mater. Phys.*, 2000, **61**, 14095.
37 K. Erickson, R. Erni, Z. Lee, N. Alem, W. Gannett and A. Zettl, *Adv. Mater.*, 2010, **22**, 4467.
38 C. Gómez-Navarro, T. R. Weitz, A. M. Bittner, M. Scolari, A. Mews, M. Burghard and K. Kern, *Nano Lett.*, 2007, **7**, 3499.
39 K. A. Mkhoyan, A. W. Contryman, J. Silcox, D. A. Stewart, G. Eda, C. Mattevi, S. Miller and M. Chhowalla, *Nano Lett.*, 2009, **9**, 1058.
40 D. Yang, A. Velamakanni, G. Bozoklu, S. Park, M. Stoller, R. D. Piner, S. Stankovich, I. Jung, D. A. Field, C. A. Ventrice, Jr and R. S. Ruoff, *Carbon*, 2009, **47**, 145.
41 G. Eda, C. Mattevi, H. Yamaguchi, H. Kim and M. Chhowalla, *J. Phys. Chem. C*, 2009, **113**, 15768.
42 Y. W. Tan, Y. Zhang, K. Bolotin, Y. Zhao, S. Adam, E. H. Hwang, S. Das Sarma, H. L. Stormer and P. Kim, *Phys. Rev. Lett.*, 2007, **99**, 246803.
43 T. Kobayashi, N. Kimura, J. Chi, S. Hirata and D. Hobara, *Small*, 2009, **6**, 1210.